Feature Extraction-Enhanced Wavelet Transform Computation for High-Impedance Fault Detection

[1]Shyh-Jier Huang and [1]Hsing-Ho Wan

Abstract

This paper proposed a feature extraction-enhance wavelet transform computation to detect the high-impedance fault in power systems. This proposed approach starts with the feature acquisition of characteristic frequencies of faults via wavelet transform. Through the comprehension of wavelet coefficients located at characteristic frequencies, a group of diagnostic indices can be hence systematically obtained such that HIF events can be more effectively discriminated from other events. The method has been validated under different scenarios. Results help support the feasibility of the method for the HIF detection study.

Keywords: High-impedance faults, wavelet transform, feature extraction.

1. Introduction

When an overhead broken conductor fell down to high-impedance ground surfaces or contacted by foreign objects, high-impedance faults (HIFs) often occur. Because the voltage magnitude is limited while the impedance between the fault point and ground is significant, such an event may not easily be detected solely by conventional protective devices. Worst of all, since the downed or open conductors may remain energized, there exists a certain probability of causing the serious injuries or even leading to a fire hazard. Considering both public safety and quality of supplying-power, it becomes crucial important to pay attention to detecting this event.

For the past decades, the nature of this HIF has been widely studied. HIF exhibits the characteristics of low fault currents, high randomness and rich in harmonics [1]-[3]. Many techniques were successively proposed to detect this event. Some detection devices have adopted electromechanical relays or designed special schemes based on the ratio of zero-sequence to positive-sequence current [4], [5]. Other studies focused on tracking the changes in harmonic currents of feeders, by which the algorithms were developed based on even-order harmonic current [6], the third harmonic current magnitude and phase angle [7], or the energy variance of even-order harmonics [8].

Recently, with the emergence of computational intelligence, some intelligent approaches were subsequently suggested to cope with this HIF problem. Test methods may include decision-tree-based methods [9], expert systems [10], fractal approach [11], and artificial neural networks method [12]. A commercial product was also reported to reach a high detection rate by using expert system-based algorithms [13]-[14]. It is worth mentioning that most of these methods utilized the Fourier transform as the main tool; however, by transforming all the information in time domain to frequency domain, relationships between time and frequency were found difficult to grasp, causing the difficulty of visualizing event dynamics. Following the advancement of wavelet transform, this method has been also applied to several applications with great appreciation. By automatically adjusting the window function to adapt to the required resolution, the wavelet transform method excels at exhibiting the time and frequency information simultaneously [15]-[18]. This approach was employed for HIF detection as well, where the absolute sum value of wavelet coefficients was served for the performance evaluation, yet the physical meaning is still vague [16]. A pattern recognition approach was hence proposed, where either root-mean-squared voltage and current or the phase displacement between zero-sequence voltage and current were acted as the classifier [17]-[18]; however, its time-consuming task

Corresponding Author: Shyh-Jier Huang
(E-mail:clhuang@mail.ncku.edu.tw)
[1]*Department of Electrical Engineering*
National Cheng Kung University
Tainan, Taiwan 70101

of measurements along with the cost of hardware implementation may offset the economical values of the method.

In this paper, a feature extraction-enhanced wavelet transform is proposed to accomplish the HIF detection. The research begins with concentrating on the dynamics of line currents acquired at characteristic frequency under HIFs and normal conditions. Then, through the wavelet transform computation, those significant components of HIF currents will be effectively comprehended, and distinctive features of HIFs are meanwhile revealed. Next, by those wavelet coefficients located at corresponding frequencies of faults, the proposed approach would formulate a diagnostic indices as an aid to detect the HIF event. While this approach effectively reflects the nature of arcing phenomenon through the extracted feature, it is also noted that only a limited number of input current sensors are required for the computation, thereby reducing the complexity of hardware realization and saving the investment cost. Features of this method are threefold:

1). It is effective to monitor the occurrence of HIFs. Whenever the signal comes with a drastic change, the method is capable of zooming in the area of interest for a clearer visualization.

2). It is useful to assimilate both time and frequency information in an integrated scheme, further facilitating the circuit realization of a forewarning mechanism.

3). The method is beneficial to analyze those non-stationary signals. It owns the potential of extending to supervise other kinds of disturbances.

The organization of this paper is made as follows. Section II introduces the paradigms of the proposed approach, Section III investigates the feature extraction and wavelet computation, Section IV discusses the numerical tests under different scenarios, and Section V draws the conclusions.

2. Paradigms

To formulate the paradigm of HIF, a three-phase, four-wire, 60 Hz distribution system of a utility was first examined. Fig.1 (a) shows a one-line diagram consisting of a 161/22.8 kV substation and two 10-kM overhead lines, where a 1500 kVA capacitor bank is employed as a reactive power compensator. As the figure depicts, when the switch S1 is off and S2 is on, it simulates the scenario where the feeder falls down to the ground surface. Then, when both S1 and S2 are on, it simulates the case when the conductor contacted by foreign objects. Only with the case of switch S2 off and S1 on, does the system operate in a normal state. At this time, if switch S3 is on, it is used to evaluate the scenario of capacitor bank switching.
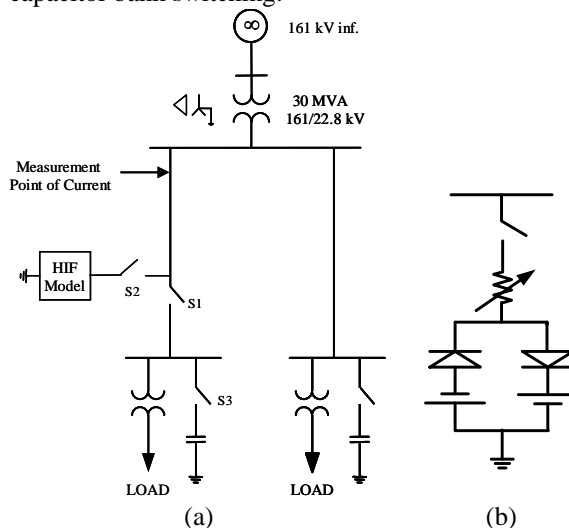

Figure 1: (a) Schematic diagram of the simulated power (b) High impedance fault model

Now, in order to investigate the HIF characteristics, Fig. 1(b) shows an arcing fault model [19], where a non-linear resistor representing the varying resistance of HIF is adopted. In this model, the DC voltage source represents the threshold voltage of the spark gap. When the feeder voltage is larger than the positive DC voltage or smaller than the negative DC voltage, arc fault currents would appear. Yet, if the feeder voltage is situated between positive and negative threshold, there will be no fault current observed. For every half cycle, magnitudes of non-linear resistor and two DC sources are simulated to change randomly, hence allowing for better assessment of asymmetrical fault that may occur

under different ground surfaces. Fig. 2 delineates the waveform, where the relationships between simulated feeder voltage and arc current are plotted. This figure helps confirm the consistence between the model and HIF paradigm, reaching a good agreement with the measured HIF waveform as shown in [1].
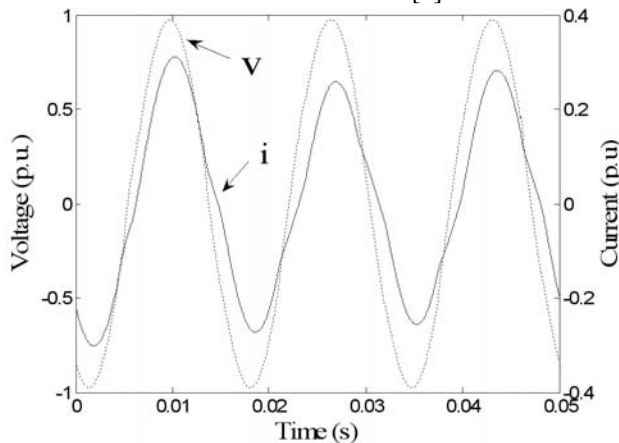

Figure 2: Relationship of arc current and feeder voltage (solid line: arc current, dashed line: feeder voltage)

Next, considering the multi-resolution capability exhibited by wavelet transform where each frequency component at an appropriate time resolution can be efficiently comprehended, a wavelet transform is first motivated for this application. Then, due to the complexity reduction capability of feature extraction technique, such technique was further added to enhance the visualization capability of the method. Therefore, a system that integrated the feature extraction with the wavelet transform is proposed in this study, in which there are three detection modes included. They are detection of characteristics waveform, detection of high-frequency indices, and detection of low-frequency indices. The main purpose behind this design was to justify the degree of difference on time-frequency plane through the wavelet transform presentation, thus paving the road to improve the detection performance.

3. Feature extraction and wavelet computation

Based on the concept discussed above, the wavelet analysis was applied to extract characteristic frequencies in a systematic way. These frequencies F_i can be determined as follows:

$$F_i = \frac{F_{ci}}{a \cdot T_s} \tag{1}$$

where F_{ci} is the center frequency of the i-th wavelet in Hz, a is the scale factor of wavelet transform, and T_s is the sampling period of the input signal. Now that the HIF signals are often located at frequency of 2-10 kHz when arcing faults take place [22]-[23], the frequency ranges from 2 kHz to 10 kHz was selected as high characteristic one. In the same time, the band of 20-60 Hz was assigned as low characteristic one.

To confirm the representatives of these characteristics frequencies, Fig. 3(a)-(c) individually shows time-frequency representations under normal, foreign contact, and downed conductor conditions, where the horizontal axis represents the sampled points (time), the vertical axis the scale (frequency), and the color density the magnitude of wavelet coefficients. From these plots, the irregular distribution and a brighter color were clearly seen at the frequency lower than the fundamental one in Fig. 3(b) and (c), implying that wavelet coefficients distributed at 20-60 Hz have presented drastic changes.
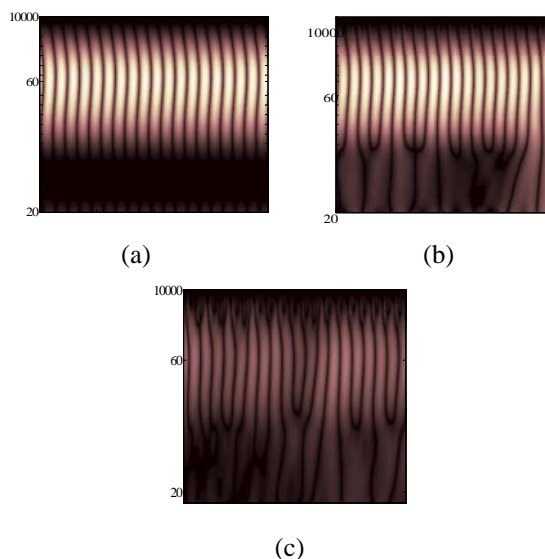

(a)　　　　　　　　　　(b)

(c)

Figure 3: Time-frequency planes (a) normal (b) foreign contact (c) downed conductor.

Next, as shown in Fig. 4, the proposed algorithm is ready to compute the norm values of wavelet coefficients located at those frequencies. In the computation, the threshold for the time duration was selected to be 8 cycles. This length of duration was decided because the average duration of HIFs was reported to be about 8 cycles [1]. Hence, through the vector form of $X = [x_1, x_2, x_3 \cdots x_n]$ organized by each wavelet coefficient, the l2-norm can be computed [21]:

$$Norm = \sqrt{x_1^2 + x_2^2 + x_3^2 + \cdots + x_n^2} \qquad (2)$$

where n is the number of wavelet coefficients during 8 cycles. This computed norm can be used to measure the Euclidean length of various signals located at characteristic frequencies of fault, serving as a quantitative measure for HIF diagnosis. The reason of using this method is supported by two features; one lies in that wavelet coefficients of fault current are more significant than that of non-fault one, the other exists in that the norm of HIF current becomes larger when the fault happens. Based on these distinctive features, a normalized variation ratio (VR) can be computed:

$$VR(\%) = \frac{N - N_{norm}}{N_{norm}} \times 100\% \qquad (3)$$

where N_{norm} and N are the norm value of non-fault and fault condition, respectively. This normalized variation ratio represents the degree of norm variations for the event considered. The higher the ratio, the more significant discrimination the selected wavelet basis function will reach.
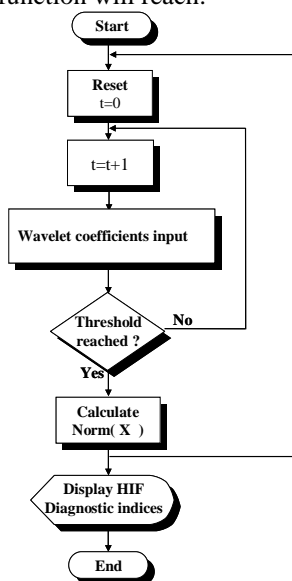

Figure 4: Flowchart of wavelet computation

Table 1 lists the computed norm obtained under normal and foreign contact conditions. The wavelet basis functions considered here includes Daubechies (db3), Gaussian, symmetry, Mexican Hat, Meyer, and Haar wavelets. From tabulated values, Daubechies wavelet function was found to possess a highest variation. Therefore, the db3 basis function was selected for this study.

Table 1: Computed norm of different wavelet bases

Wavelet Basis	Normal Condition	Foreign Contact	VR (%)
Daubechies (db3)	0.0168	0.0992	490.47
Gaussian	0.0243	0.0861	254.32
Symmetry wavelet	0.1575	0.2384	51.36
Mexican hat	0.2724	0.4077	49.66
Meyer	0.1414	0.1876	32.67
Haar wavelet	5.1777	6.7991	31.31

4. Test results

To validate the effectiveness of this proposed approach, it has been tested through simulated events. Test scenarios considered are listed below:

1). Downed conductor: an overhead conductor that is broken and downed to a high-impedance surface;

2). Contacted by foreign object: a bare conductor is contacted by foreign object such as trees.

For both tests, signals were sampled at the rate of 25 kHz. A total of 11 load conditions were investigated. By employing the fault model of Fig. 2, HIF events were assumed to occur at the point as indicated in Fig. 1 (a). The load level ranged from 60% to 110% of full load with a 5 % step, where the power factor was 0.8 lagging. Each HIF event and foreign contact was individually tested five times at different load levels. Therefore, the number of tested case amounts to 110 ($11 \times 5 \times 2 = 110$). Under different load conditions, capacitor banks were switched on/off once, by which there are 22 test cases of capacitor bank-switching. For all of these cases, two DC voltage sources for the HIF model were randomly selected from 3 kV to 10 kV, and the phase of 161 kV source was either 0° or 90°. Test results using the proposed approach under different scenarios are discussed below.

1). Downed Conductor

Fig. 5(a) shows the current waveform, in which the conductor was downed to the ground at 50 ms. Fig. 5(b) shows the contour plot of wavelet coefficients distributed at the frequency of 2-10 kHz in time-frequency plane. As seen from this plot, those wavelet coefficients at the pre-fault stage were insignificant. Yet, once an HIF took place, variations of coefficients became observable, indicating a sufficient distinction to justify fault scenarios. At this time, by comparing Fig. 5(b) with Fig. 5(a), the distribution of wavelet coefficients was clearly seen in good agreement with the occurrence and disappearance of arcing-fault transients at every half cycle, further validating the proposed method for the scenario assumed.

For the subsequent analysis of diagnostic indices, a frequency of 2 kHz was also chosen as high characteristic frequency based on the plot of Fig. 5 (b). This selection of low characteristic frequency will be detailed later.
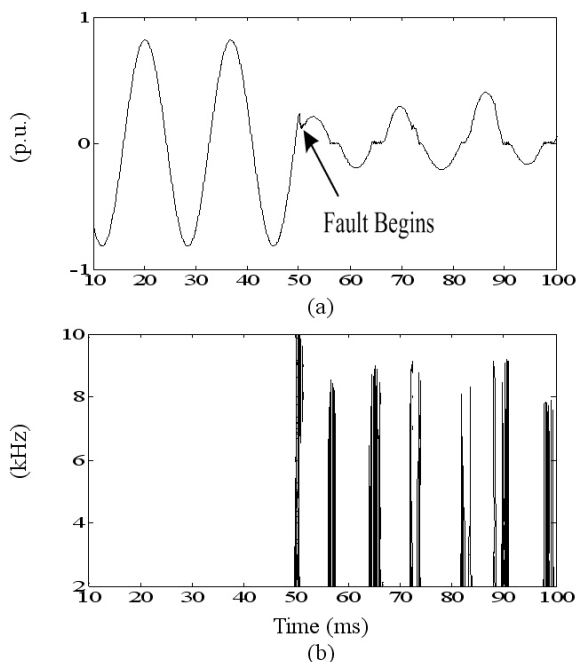
2). Foreign Contact

In this case, the scenario of foreign contact is examined. Fig. 6 (a) shows the current waveform at R-phase, where the conductor was contacted by foreign objects at 50 ms. Since this conductor is unbroken, the current variation is limited. Fig. 6 (b) plots the contour plot of distribution of wavelet coefficients in the range of 2-10 kHz. As shown in the figure, wavelet coefficients obtained from pre-fault current are considerably small. However, when an HIF event occurs, these coefficients would exhibit a significant increase that is quite different from the pre-fault condition, offering a convenient way of fault discrimination. Note that in this case, a high characteristic frequency of 2 kHz can be simultaneously observed.
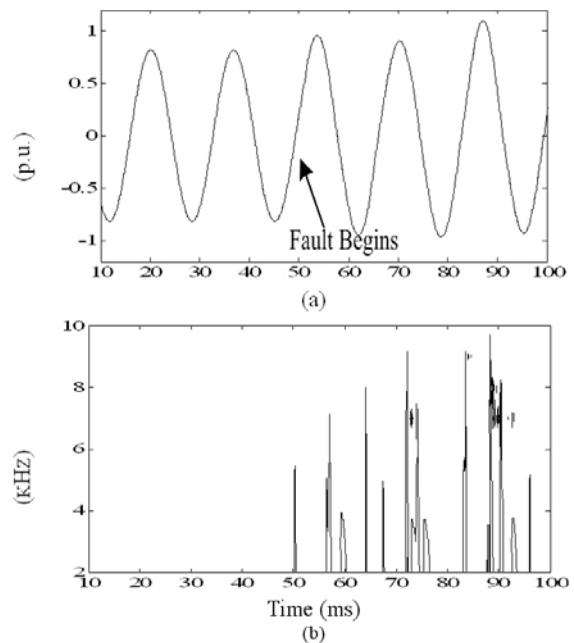
Figure 6: Foreign contact in R-phase feeder. (a) Current waveform. (b) Wavelet coefficients in the range of 2-10 kHz.

Figure 5: A downed conductor in R-phase feeder. (a) The current waveform. (b) Wavelet coefficients in the range of 2-10 kHz.

3). Capacitor-Switching

In order to discriminate the capacitor-switching from the HIF fault, this case investigated a scenario where a switching of three-phase 1500 kVAR capacitor bank happened at 65% of full load. In the case, this capacitor bank was energized at 50 ms and then de-energized at 150 ms. The switching occurs at an inception angle of 0° of voltage source. It was found that the amplitudes of transients due to capacitor-switching can be greater than that of capacitor nominal current. Fig. 7 (a) shows the R-phase current waveform, and Fig. 7 (b), plots its corresponding contour of wavelet coefficients distributed in the range of 2-10 kHz. As Fig. 7 (b) delineates, a sudden increase of wavelet coefficients happened only at the instant when the switching was made. This phenomenon is different from aforementioned two HIF cases, by which the capability of discriminating a switching event from HIFs is confirmed.
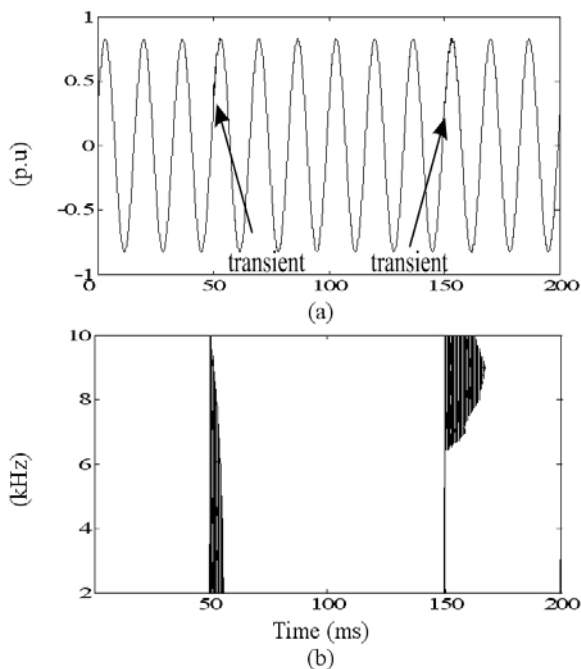

Figure 7: Capacitor-switching. (a) R-phase current waveform. (b) Wavelet coefficients in the range of 2-10 kHz.

4). Diagnostic Indices

In addition to aforementioned analysis, this study has examined the diagnostic indices formed by each considered event. These diagnostic indices can be obtained by computing the norm detailed in Section III. Fig. 8 and 9 show the results of high-frequency diagnostic indices computed based on the characteristic frequency of 2 kHz, where indices at each phase are all illustrated. Fig. 8 (a) and (b) individually plots the test results of downed conductor and foreign contacts. They have shown that when any HIF takes place at a certain phase (for example, R-phase), its corresponding index would be higher than others. Hence, a sudden raise of high-frequency diagnostic indices can be a useful indicator to the occurrence of event.

Fig. 9 (a) and (b) illustrate the results of capacitor bank switching energized and de-energized. It delineates the random distribution of indices obtained at the first 8-cycle window. Because the transients merely last for a short period, indices for three phases have decreased rapidly, which is significantly different from HIFs events.
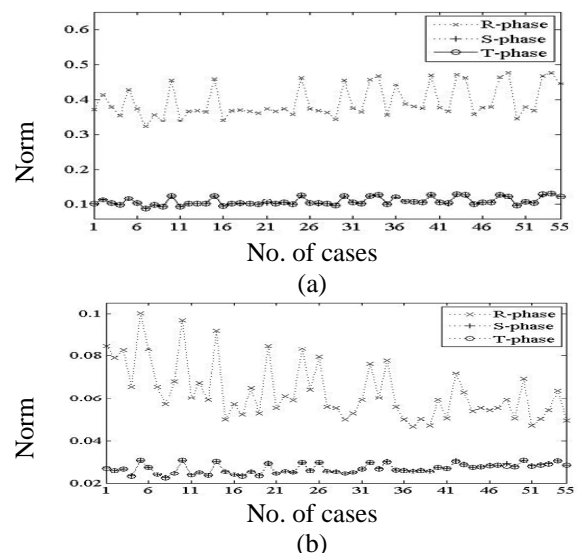

Figure 8: High-frequency diagnostic indices for HIFs. (a) A downed conductor in R-phase feeder. (b) Foreign contact in R-phase feeder
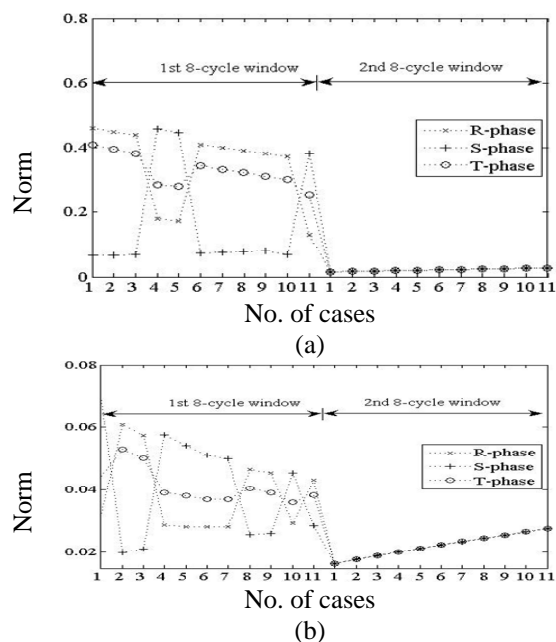
(a)

(b)

Figure 9: High-frequency diagnostic indices for capacitor bank switching. (a) Capacitor bank is energized. (b) Capacitor bank is de-energized.

(a)

(b)

(c)

Figure 10: Wavelet coefficients of low frequency. (a) Normal condition. (b) Foreign contact in R-phase feeder. (c) Broken feeder in R-phase feeder

Next, in the investigation of low-frequency indices, a longer observation is required for the adequate extraction. Based on the time-frequency plot depicted in Fig. 3 as well as intrinsic differences observed between healthy and fault cases, a frequency band of 20-60 Hz was chosen as the low characteristic frequency.

Fig. 10 shows the contour plot of wavelet coefficients distribution of low frequency obtained under normal operation, broken feeder and foreign contact. Unlike high frequency features shown in Fig. 5 (b), 6 (b) and 7 (b) where variations of coefficient come with a distinctive change, the features obtained with low frequency are less significant. This implies that the low-frequency diagnostic indices for HIFs may be insufficient to be distinctive. It is also worth noting that, in order to ensure a higher security, a longer duration of observation may be necessary because the transients under a normal scenario would merely appear for a very short period, whereas the occurrence of HIF would last a longer period.
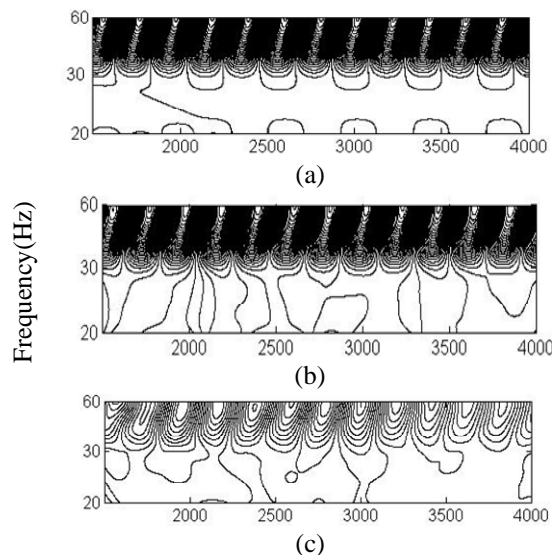
5. Conclusions

In this paper, an approach is proposed to enhance the high-impedance fault detection performance. By an appropriate selection of features as well as an inspection of indices variation, it provided a systematic way of discriminating between HIF and switching events. Through tested scenarios of downed conductor and foreign contact, the method effectively demonstrated its high potential for the HIF detection. This approach also owns a high potential of further developing to visualize other disturbances.

References

[1] Detection of Downed Conductors on Utility Distribution Systems, *IEEE Tutorial Course*, 90EH0310-3-PWR, 1989.

[2] A. F. Sultan, G. W. Swift and D. J. Fedirchuk, "Detecting arcing downed-wires using fault current flicker and half-cycle asymmetry," *IEEE Transactions on Power Delivery*, vol. 9, no. 1, pp. 461-470, Jan. 1994.

[3] H. Y. Chu, M. T. Chen, C. L. Huang, S. L. Chen and S. S. Yen, "High impedance fault tests on the Taipower primary distribution system," *Electric Power System Research*, vol. 19, pp. 105-114, 1990.

[4] H. Calhoun, M. T. Bishop, C. H. Eichler, and R. E. Lee, "Development and testing of an electro-mechanical relay to detect fallen distribution conductors," *IEEE Transactions on Power Apparatus and Systems*, vol. 101, pp. 1643-1650, June 1982.

[5] R. E. Lee and M. T. Bishop, "Performance testing of the ratio ground relay on a four-wire distribution feeder," *IEEE Transactions Power Apparatus and Systems*, vol. 102, pp. 2943-2949, Sep. 1983.

[6] W. H. Kwon, G. W. Lee, Y. M. Park, M. C. Yoon and M. H. Yoo, "High impedance fault detection utilizing incremental variance of normalized even order harmonic power," *IEEE Transactions on Power Delivery*, vol. 6, no. 2, pp. 557-564, Apr. 1991.

[7] D. I. Jeerings and J. R. Linders, "A practical protective relay for down-conductor faults," *IEEE Transactions on Power Delivery*, vol. 6, no. 2, pp. 565-574, Apr. 1991.

[8] K. Y. Lien, S. L. Chen, C. J. Liao, T. Y. Guo, T. M. Lin, and J. S. Shen, "Energy variance criterion and threshold tuning scheme for high impedance fault detection," *IEEE Transactions on Power Delivery*, vol. 14, no. 3, pp. 810-817, July 1999.

[9] Y. Sheng and S. M. Rovnyak, "Decision tree-based methodology for high impedance fault detection," *IEEE Transactions on Power Delivery*, vol. 19, no. 2, pp. 533-536, Apr. 2004.

[10] B. D. Russell and C. L Benner, "Arcing fault detection for distribution feeder: security assessment in long term field trials," *IEEE Transactions on Power Delivery*, vol. 10, no. 2, pp. 676-683, Apr. 1995.

[11] A. V. Mamishev, B. D. Russell, and C. L. Benner, "Analysis of high impedance fault using fractal techniques," *IEEE Transactions on Power Systems*, vol. 11, no. 1, pp. 435-440, Feb. 1996.

[12] A. S. Bretas, M. Moreto, R. H. Salim, and L. O. Pires, "A Novel High Impedance Fault Location for Distribution Systems Considering Distributed Generation, *IEEE Transmission and Distribution Conference and Exposition: Latin America*, Caracas, Venezuela, pp. 1-6, August 2006.

[13] High Impedance Fault Detection Technology, PSRC Working Group D15, 1996.

[14] F60 Feeder Management Relay UR Series Instruction Manual, GE Multilin, 2006.

[15] S. J. Huang and C. T. Hsieh, "High-impedance fault detection utilizing a Morlet wavelet transform approach," *IEEE Transactions on Power Delivery*, vol. 14, no. 4, pp. 1401-1410, Oct. 1999.

[16] V. Torres, and P. H. F. Ruiz, "High Impedance Fault Detection Using Discrete Wavelet Transform", *IEEE Electronics, Robotics and Automotive Mechanics Conference,* Morelos, Mexico, pp. 325-329, November 2011.

[17] T. M Lai, L. A. Snider, E. Lo, and D. Sutanto, "High-impedance fault detection using discrete wavelet transform and frequency range and RMS conversion," *IEEE Transactions Power Delivery*, vol. 20, no. 1, pp. 397-407, Jan. 2005.

[18] M. Michalik, W. Rebizant, M. Lukowicz, S.J. Lee, and S.H. Kang, "High impedance fault detection in distribution networks with use of wavelet-based algorithm," *IEEE Transactions on Power Delivery*, vol. 21, no. 4, pp. 1793-1803, Oct. 2006.

[19] A. E. Emanuel, D. Cyganski, J. A. Orr, S. Shiller, and E. M. Gulachenski, "High impedance fault arcing on sandy soil in 15 kV distribution feeders: Contributions to the evaluation of the low frequency spectrum," *IEEE Transactions on Power Delivery*, vol. 5, no. 2, pp. 676-686, Apr. 1990.

[20] I. Daubechies, *Ten Lectures on Wavelets*. Philadelphia, PA: Soc. Industrial Appl. Math., 1992.

[21] http://www.ugrad.cs.ubc.ca/~cs402/handouts/handout03.pdf

[22] M. Aucoin, B. D. Russell, and C. L. Benner, "High impedance fault detection for industrial power systems," *IEEE Industry Applications Society Annual Meeting*, San Diego, USA, vol. 2, pp. 1788–1792, October 1989.

[23] M. S. Ali, A. H. A. Bakar, H. Mokhlis, H. Aroff, H. A. Illias, and M. M. Aman, "High impedance fault localization in a distribution network using the discrete wavelet transform", *IEEE International Conference on Power Engineering and Optimization*, Kuala Lumpur, Malaysia, pp. 349 – 354, June 2012.